THE JOURNAL OF PHYSICAL CHEMISTRY C

Article

pubs.acs.org/JPCC

Probing Lithiation Kinetics of Carbon-Coated $ZnFe_2O_4$ Nanoparticle Battery Anodes

Fernando Martinez-Julian,[†] Antonio Guerrero,[†] Marta Haro,[†] Juan Bisquert,[†] Dominic Bresser,[‡] Elie Paillard,[‡] Stefano Passerini,[‡,§] and Germà Garcia-Belmonte*[,†]

[†]Photovoltaics and Optoelectronic Devices Group, Departament de Física, Universitat Jaume I, 12071 Castelló, Spain

[‡]Institute of Physical Chemistry & MEET Battery Research Centre, University of Muenster, Corrensstr. 28/30 & 46, 48149 Muenster, Germany

[§]Helmholtz Institute Ulm, Karlsruhe Institute of Technology, Albert-Einstein-Allee 11, 89081 Ulm, Germany

ABSTRACT: The investigation of the lithiation−delithiation kinetics of anodes comprising carbon-coated $ZnFe_2O_4$ nanoparticles is reported in here. The study confirmed that, as occurring with other conversion electrodes, lithiation of $ZnFe_2O_4$ nanoparticles is a multistep process involving the presence of intermediate Li−Zn−Fe−O phases as precursors for the formation of amorphous Li_2O. A detailed knowledge on the reaction kinetics of the involved electrochemical mechanisms has been achieved by using impedance spectroscopy. It has been observed that lithiation reactions introduce a long delay that limits the electrode charging, not related to diffusion mechanisms. The sloping curve following the conversion plateau of the galvanostatic discharge is connected to a retardation effect in the reaction kinetics. This limitation is seen as an additional resistive process originated by the specific lithiation microscopic features. It is concluded that capacitance spectra allow distinguishing two separate processes: formation of kinetically favored intermediate Li−Zn−Fe−O phases and subsequent reaction to produce highly dispersed LiZn and Fe^0 in an amorphous Li_2O matrix. A detailed electrical model is provided accounting for the overall electrode lithiation process.

INTRODUCTION

Li-ion batteries have become core devices for the consumer electronics industry. Materials for commercial battery electrodes are mostly chosen from a set of intercalation compounds that reversibly accommodate lithium ions in host sites in the lattice without severely distorting the structure. In most transition metal compounds such as $LiCoO_2$, $LiNi_{1-y-z}Mn_yCo_zO_2$, $LiFePO_4$, and $Li_4Ti_5O_{12}$, redox activity is restricted to a few exchanged electrons. Therefore, intercalation materials exhibit intrinsic limitations that make them unviable when high capacity requirements have to be fulfilled as in the case of large scale or automotive applications.[1−3] During the past decades a new family of electrode materials operating under the so-called conversion reaction has been intensely studied.[4] For these compounds lithiation occurs through the reaction that involves a complete metal reduction as $M_aX_b + (bn)Li \leftrightarrow aM + bLi_nX$, where M = transition metal, X = anion (O, S, N, P, and F), and n = anion formal oxidation state. Conversion reaction is able to accommodate larger amount of Li atoms into the lithium binary compound Li_nX, which explains specific capacities exceeding 1000 mAh g^{-1} as reported for many compounds. Interestingly, conversion materials usually show good reversibility because of the formation of a nanostructured matrix that comprises metallic nanoparticles surrounded by amorphous Li_nX phases. Intimate phase contact facilitates reactivity as evidenced by the observation of remaining metallic nanoparticles after extended oxidation/reduction cycling.[4] Despite their potentialities, conversion compounds present a series of performance limitations that hinders their straightforward application in commercial devices. There is a strong structural rearrangement concomitant to the chemical reaction, usually accompanied by material decohesion and cycling performance loss. A large Coulombic inefficiency is often observed in the first cycle, and a voltage hysteresis, that in some cases even exceeds 1 V, precludes incorporation into commercial batteries.[5] In addition to conversion materials, other reactions of interest include Li alloying with metal and semimetal atoms which are able to give very high capacities, although showing problems related to large volume changes during the dealloying process.

An important research effort during the past decade has allowed progressing into the understanding of the conversion reaction mechanism. Structural and chemical changes have been monitored by means of several spectroscopic techniques such as transmission electron microscopy (TEM), electron energy-loss spectroscopy (EELS),[6] X-ray diffraction (XRD),[7] and solid-state nuclear magnetic resonance (NMR).[5] In most cases, it has been identified that the electrochemical mechanism for the transformation of the pristine M_aX_b phase into Li_nX and metallic particles is a multistep process that entails the

Received: December 26, 2013
Revised: March 3, 2014
Published: March 7, 2014

   dx.doi.org/10.1021/jp412641v | J. Phys. Chem. C 2014, 118, 6069−6076

intermediate formation of ternary Li−M−X phases before such conversion takes place. The fluorides/oxides also exhibit additional reversible capacity at lower voltages beyond their theoretical capacity through mechanisms that are still poorly understood. Although evident progress in structural and thermodynamic processes underlying lithiation of conversion materials has been achieved, a detailed knowledge on the conversion (and related reactions) kinetics would help having a complete picture on the electrochemical mechanisms accompanying the inherent structural rearrangements. In condensed matter, the reaction rate is largely affected by strong interactions caused by phase transitions and rearrangements.[8] Despite inherent complex thermodynamics, electrode kinetic limitations are commonly connected to the solid-state diffusion of ionic and electronic species. This is the case of intercalation compounds that exhibit a charging hindrance connected to a delay in the ion uptake caused by the Li^+ transport in the host material. However, we have pointed out recently[9] that solid-state reactions as those occurring in conversion and alloying electrodes can produce an intrinsic delay linked with the reaction mechanism itself. This is then the specific aim of this work: how to extract kinetic information on the lithiation mechanisms occurring in a highly reversible zinc ferrite nanoparticle battery electrode.

Zinc ferrite electrodes are selected in this work because they exhibit large specific capacity (>1000 mAh g^{-1}) while maintaining rather good kinetic performance upon charge/discharge high rate response.[10] This is achieved by carbon coating $ZnFe_2O_4$ nanoparticles, resulting in an amorphous carbon shell covering them. This procedure assures specific capacities of ca. 1000 mAh g^{-1} for low specific currents, which is more than 5 times the specific capacity obtainable for standard anodes as $Li_4Ti_5O_{12}$(LTO). At rates as high as 1 A g^{-1} only about 10% of the low-rate specific capacity is lost, and the rate advantage is preserved when compared to nanoparticulate LTO.[3,10] Carbon coating improves significantly not only the high rate capability of the resulting electrodes but also the cycling stability as well as the capacity retention after the applied C rate test. Comparing the discharge voltage profiles for carbon-coated $ZnFe_2O_4$−C and uncoated $ZnFe_2O_4$, an important reduction of the initial voltage drop is observed at elevated C rates for the former material. Additionally, the carbon coating is observed to enhance the electrode kinetics by ensuring electron supply to the nanoparticles.[10] This good rate performance suggests us that ion diffusion cannot be regarded as a limiting process of the electrode kinetic response and that $ZnFe_2O_4$−C based anodes are proper candidates to explore the kinetics of the lithiation mechanisms avoiding diffusion hindrance.

Lithiation kinetics will be probed here by means of electrochemical impedance spectroscopy (EIS). This technique directly faces the kinetics of the electrical response of those mechanisms governing the change in the electrode state of charge. We have identified in this work, by using EIS, that lithiation reactions in conversion materials introduce a long delay that limits the electrode charging. This limitation is seen as an additional resistive process originated by the specific features of the microscopic lithiation mechanism. Combined with the large capacitive process caused by the electrode charging, the reaction resistance yields a distinctive signature in the imaginary part of the capacitive spectra. As a result, it is feasible to extract a reaction frequency that establishes the time scale at which the particular solid-state reaction occurs. The analysis of the impedance/capacitance response of conversion electrodes performed here opens new room for understanding kinetic features of the lithiation process that are usually hidden by relying exclusively upon structural characterization techniques.

EXPERIMENTAL RESULTS

Electrochemical Response. Preparation procedure and electrochemical response of $ZnFe_2O_4$−C nanoparticle anodes have been fully addressed in previous work.[10] A two-electrode Swagelok cell assembly with lithium metal as the counter/reference electrode was used. The setup includes a Whatman grade GF/C 260 μm thick as the separator, and the electrolyte solution obtained by dissolving 1 M $LiPF_6$ into a mixture of ethylene carbonate (EC) and dimethyl carbonate (DMC) (EC/DMC, 50:50 w/w). Three first cyclic voltammograms at scan rate 0.05 mV s^{-1} can be observed in Figure 1a. Remarkably, the voltammogram does not change significantly upon further sweeps, confirming a highly reversible uptake and release of lithium once the initial structural changes are completed. After the first scan a large reduction (cathodic) peak is exhibited at approximately 1.0 V, which was interpreted in terms of the main conversion reaction as $Zn_xFe_yO + 6Li^+ + 6e^- \rightarrow Zn^0 + 2Fe^0 + 3Li_2O$. By means of this reaction, previously formed oxide phases resulting from intermediate Li−Zn−Fe−O compounds are transformed into metallic Zn and Fe and Li oxide. A minor shoulder around 1.2 V is believed to be related to the formation of intermediate ternary phases including Zn and Fe, with Li and O of different compositions. Anodic current shows a maximum at 1.6 V during the oxidation stage. It has been also proposed that, at lower cathodic potentials, an alloying reaction involving Zn and Li takes place as $Zn^0 + Li^+ + e^- \rightarrow LiZn$. This additional reaction would explain the increment in the specific capacity below 0.8 V. In summary, the electrode behavior can be assimilated to a typical

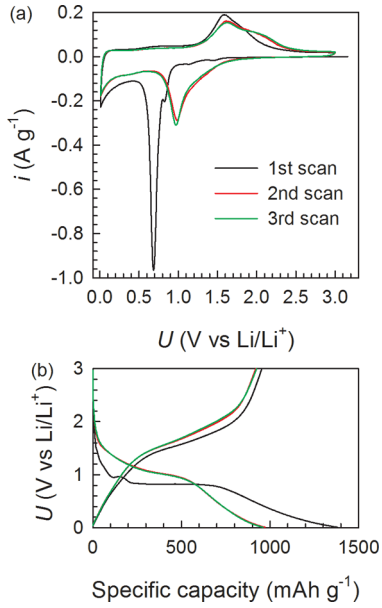

Figure 1. (a) Cyclic voltammogram of a $ZnFe_2O_4$-C (13.05 wt % C)/SuperC65/CMC (75/20/5) electrode at 0.1 mV s^{-1} showing the stable response after the first cycle. (b) Voltage profile of the galvanostatic cycle of a $ZnFe_2O_4$-C electrode at 40 mA g^{-1} C/20 rate (first cycle at 20 mAh g^{-1} C/40 rate).

dx.doi.org/10.1021/jp412641v | J. Phys. Chem. C 2014, 118, 6069−6076

conversion mechanism including an additional alloying reaction with Zn and that can be viewed as $ZnFe_2O_4 + 9Li^+ + 9e^- \rightarrow LiZn + 2Fe^0 + 4Li_2O$.[10]

As observed in Figure 1a, the first scan yields a distinctive curve caused by the general structural rearrangement of the electrode material. A detailed analysis of the phase transitions was published based on in-situ XRD measurements upon initial galvanostatic lithiation−delithiation.[10] That analysis confirmed the formation of intermediate Li−Zn−Fe−O compounds that finally produce metallic Zn and Fe and amorphous Li oxide. Upon delithiation, the materials remain amorphous or, at least, quasi-amorphous, meaning that the resulting crystalline grains are simply too small to be detected by means of XRD, in common with other conversion compounds.[11,12] After the subsequent delithiation sweep the formation of amorphous ZnO and Fe_2O_3, or even $ZnFe_2O_4$, appears likely as observed for other transition metal ferrites as $CoFe_2O_4$ or $NiFe_2O_4$ using ^{57}Fe Mössbauer spectroscopy that revealed the complete reoxidation of Fe^0 to Fe^{3+}.[13,14] Although the definite structural composition in the charged (delithiated) state is not yet fully understood,[15,16] the previous arguments leads us to propose in Figure 2 the main reactions involved in the lithiation−delithiation of the zinc ferrite nanoparticles.

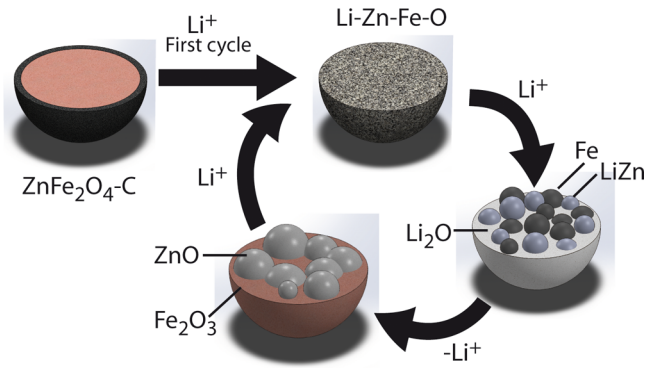

Figure 2. Schematic representation of the main processes occurring in the carbon coated $ZnFe_2O_4$-C nanoparticle. The first lithiation produces a sort of intermediate Li−Zn−Fe−O phases that evolve to the final structure comprising Fe^0 and LiZn immersed into an amorphous Li_2O matrix after conversion alloying. Delithiation sweep most likely produces the formation of ZnO and Fe_2O_3.

Galvanostatic charge−discharge test for $ZnFe_2O_4$-C electrodes within the voltage range 0.0−3.0 V vs Li/Li^+ at a rate of 0.04 A g^{-1} can be seen in Figure 1b after the first scan. As expected, a plateau is observed at potentials around 1.0 V, signaling the occurrence of the conversion reaction with the formation of metallic Zn and Fe nanoparticles and the oxide Li_2O. At lower charge states, cell voltage decreases steeply, thus indicating that the formations of intermediate phases comprising Li−Zn−Fe−O are both energetically and kinetically favored. At potentials below 0.5 V an increment in the specific capacity appears as a tail with respect to the conversion-related plateau. This additional capacity is believed to be linked with the aforementioned alloying reaction of Li with metallic Zn. Full information about the electrochemical behavior and structural characteristics of zinc ferrite electrodes can be seen in a previous work.[10]

Impedance and Capacitance Responses. EIS is performed at open-circuit voltage (no direct current flowing) in different charge states, with amplitude of 20 mV in the frequency range from 10^6 Hz down to 0.001 Hz. After the first cycle (Figure 1a), a stable cyclic voltammogram is observed which informs on the reversibility of the conversion reaction. The Nyquist plots in Figure 3 consist of two well-defined parts: the high-frequency semicircle and an inclined low-frequency line. Some of the impedance features are originated from well-known processes.[17] At high frequencies, a rather constant arc corresponds to the parallel connection between the double-layer capacitance $C_{dl} \approx 50$ μF and surface charge transfer resistance $R_{ct} \approx 25$ Ω. An additional series resistance accounts for the solution contribution $R_s \approx 12$ Ω. The high-frequency circuit elements are observed to be rather voltage independent, which allows connecting them to mechanisms occurring at the interface. The low-frequency response points to the occurrence of a voltage-modulated process which gives rise to a capacitive-like behavior. The interpretation relies on the so-called chemical capacitance that informs on the electrode ability of varying the amount c of reacted Li^+ upon application of a differential change in the chemical potential μ (directly assimilated to the electrode potential upon steady-state conditions as $\mu = qU$, where q is the positive elementary charge).[18]

$$C_\mu = q\frac{\partial c}{\partial U} \tag{1}$$

By examining Figure 3, one can infer that the impedance of the low-frequency capacitive part decreases at voltages below 1.2 V. The resistance accompanying the chemical capacitance is largely reduced in the low-voltage range, from ∼20 kΩ at 2.6 V down to 100 Ω at 0.2 V. This reduction occurring at conversion potentials signals the enhancement of the electrode charging current. For intercalation compounds the rate-limiting mechanism is the diffusion of Li^+ inside the active material.[19] Diffusion of ions gives rise to distinctive impedance patterns characterized by Warburg-like responses as $Z \propto (i\omega)^{-1/2}$ (being ω the angular frequency and $i = (-1)^{1/2}$). Models based on spatially restricted ion diffusion were proposed to account for intermediate-frequency arcs relaying on a distribution of diffusion lengths[20] or electronic transport limitations.[21] However, the electrodes analyzed in this work function by conversion reactions that entail an overall material rearrangement of both chemical and structural nature. These considerations lead us to regard the conversion reaction itself as the rate-limiting process of the change in electrode state of charge/discharge. The resistive process accompanying the chemical capacitance is seen as a manifestation of the conversion-related current hindrance.

In order to gain a deeper knowledge on the kinetics of the conversion mechanisms, we propose to show the impedance data in a representation that highlights capacitive features. Capacitance spectra are calculated from the impedance as[22]

$$C = \frac{1}{i\omega Z} \tag{2}$$

which is a complex function with its real part C' that increases toward lower frequencies, signaling the electrode charging. The imaginary part C'' is related to the inherent resistive processes that take place during the conversion reaction. Figure 4 shows the capacitive spectra corresponding to the impedance response displayed in Figure 3. As observed in Figure 4a, C' spectra exhibit a low-frequency plateau in the range of 1−10 mHz, which is interpreted in terms of the chemical capacitance in eq 1. As expected, large capacitances of ca. 0.1 F are measured

dx.doi.org/10.1021/jp412641v | J. Phys. Chem. C 2014, 118, 6069−6076

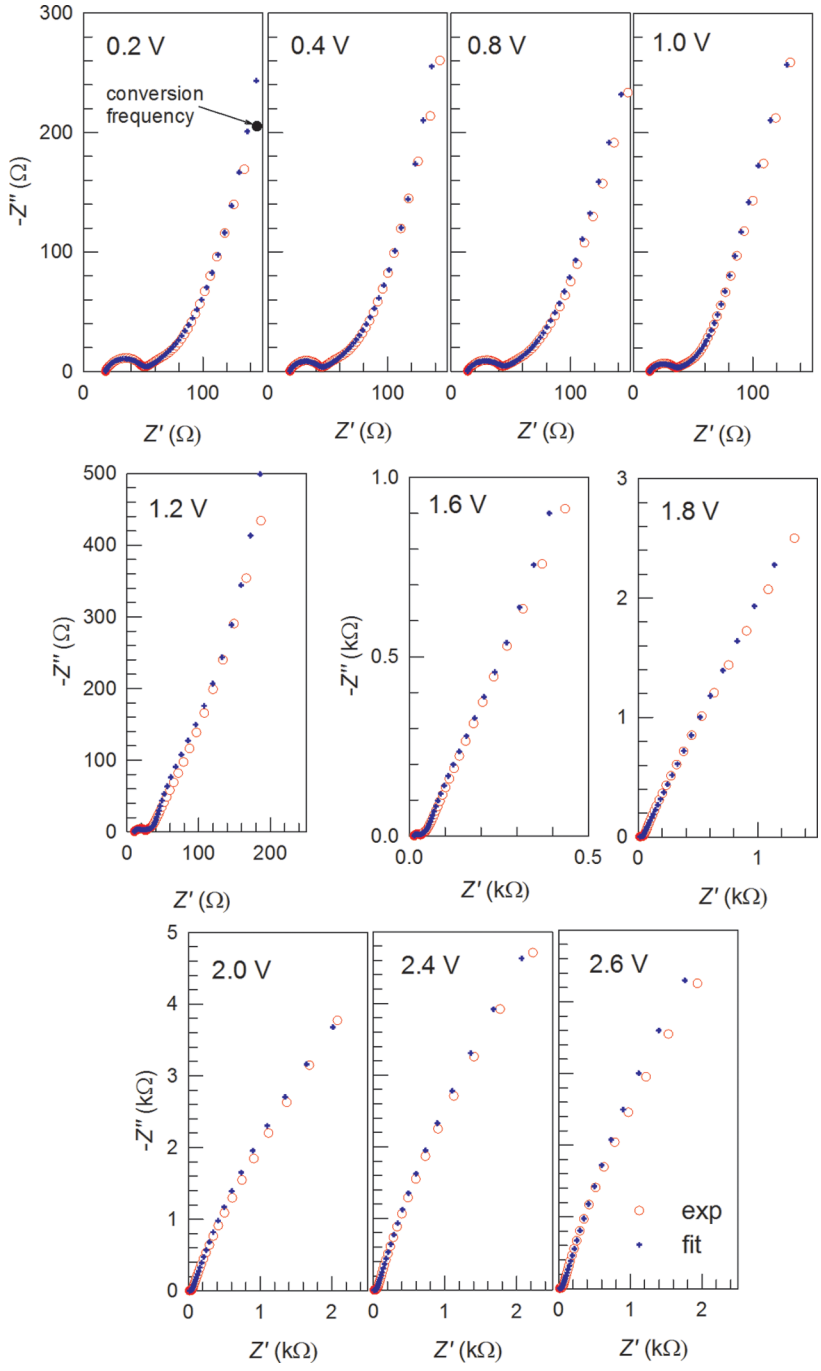

Figure 3. Impedance spectroscopy response of a $ZnFe_2O_4$-C electrode at different steady-state voltages as indicated. Experimental data and fits using the equivalent circuit of Figure 6. In the first panel, it is marked the point at the frequency corresponding to the conversion process as extracted from the capacitive analysis.

when the electrode is polarized at conversion potentials. The chemical capacitance, extracted from the low-frequency limit, increases for lower potentials in agreement with the occurrence of the conversion process. A second capacitance plateau is observed at intermediate frequencies (100 Hz−1 kHz) related to C_{dl}.

The imaginary part C'' spectra gather relevant information on the conversion kinetics. As observed in Figure 4b, C'' exhibits a peak at lower frequencies that corresponds to the inflection point in the C' step in agreement with the Kramers−Kronig relations. This peak signals a characteristic frequency (time) of the capacitive process that is confined into the low-frequency range. It is noticed that the peak height follows the increase in C' plateau. More interestingly, the characteristic frequency f_c is situated within the range of 1−10 mHz and undergoes variations with the cell potential, reaching a maximum at 1.0 V. It should be mentioned that f_c corresponds to a frequency located in the rising part of the impedance spectra in Figure 3. This entails that the underlying mechanism originating the peak in C'' is decoupled from the ac response of C_{dl} and R_{ct} circuit elements. We suggest here that the characteristic frequency encountered can be interpreted in terms of the conversion reaction kinetics as a measurement of the conversion time τ_c. An alternative representation of the capacitance data consists in

dx.doi.org/10.1021/jp412641v | J. Phys. Chem. C 2014, 118, 6069−6076

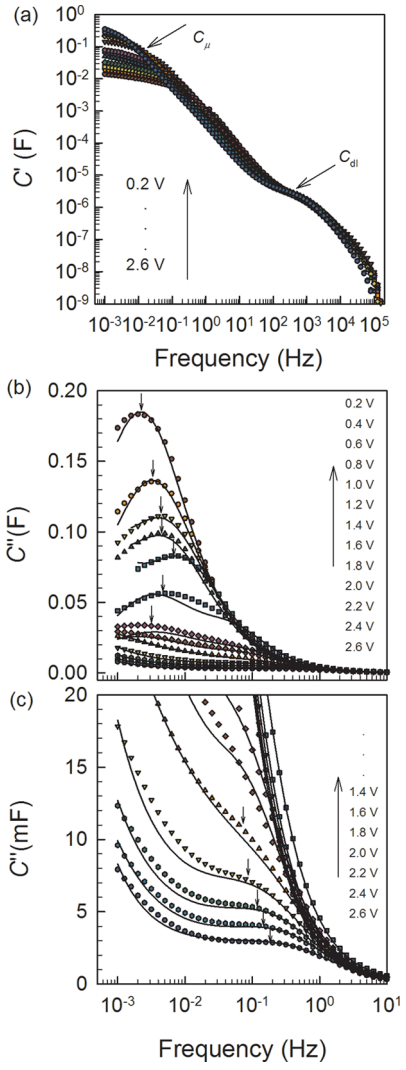

Figure 4. (a) Experimental data corresponding to the real part of the capacitance C' spectra of a $ZnFe_2O_4$-C electrode measured at different voltages. Double-layer and chemical capacitance plateaus are marked. (b) Imaginary part of the capacitance C'' spectra showing the response peak. Arrows indicate the conversion frequency. (c) Detail of C'' that allows observing a second reaction peak at higher voltages related to the formation of intermediate Li−Zn−Fe−O phases. Solid lines correspond to fitting results using the equivalent circuit of Figure 6.

plotting C'' vs C' in a complex plane as shown in Figure 5a. This kind of plot produces an arc when C'' spectra peak in such a way that each reaction mechanism can be identified. In the next section, a detailed model accounting for the equivalent circuit of the conversion impedance (capacitance) will be provided.

Because conversion is usually a multistep process involving several intermediate reactions, it is possible to observe additional reaction peaks at more positive potentials. This is indeed the case studied here. By examining C'' spectra at potentials >1.8 V, one can observe a clear peak partially masked by the response corresponding to the low-voltage C'' peak. This is displayed in Figure 4c. The high-voltage C'' process responses much faster (150−400 mHz) than the low-voltage reaction at 1−10 mHz. This secondary mechanism is also decoupled from the high-frequency interfacial response taking place at 0.1−10 kHz, and it is indeed visible in Figure 5b as a clearly distinguishable arc.

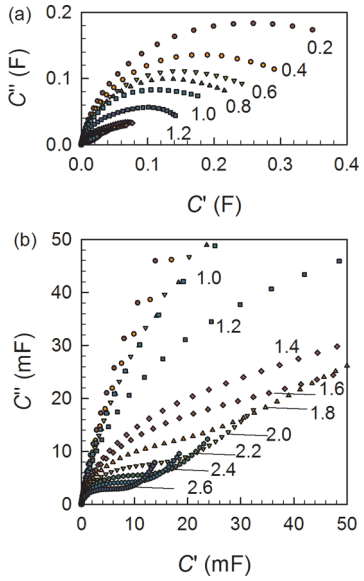

Figure 5. Experimental data corresponding to the capacitance C' plots of a $ZnFe_2O_4$-C electrode measured at different voltages (indicated). (a) Low voltage region exhibiting a differential semicircle related to the main conversion mechanism. (b) Detail of low capacitance in which a second reaction peak at higher voltages related to the formation of intermediate Li−Zn−Fe−O phases is observed.

IMPEDANCE MODEL FOR LITHIATION REACTIONS

In the previous section we have made two identifications from the experimental data: (i) The low-frequency plateau in C' spectrum is interpreted in terms of chemical capacitance. This is a steady-state value that signals the static limit of the capacitive process directly linked with the electrode charging state. (ii) The peak in C'' spectrum is connected to the kinetics of the reaction as a measurement of the conversion time τ_c. By following this approach, it is evident that impedance (capacitance) measurements simultaneously capture energetic (C' low-frequency plateau) as well as kinetic (C'' peak) aspects of the conversion process. The simplest way to model the previous features is a RC series circuit that gives a C'' peak at the characteristic time $\tau_c = RC$. This is obviously an ideal case characterized by a single conversion time. In real experiments, it is expected to be much more common to deal with distributions of conversion times as $g(\tau)$. The function accounting for capacitive response can be easily written as a distribution of RC series circuits[23]

$$C(\omega) = C_\mu \int_0^\infty \frac{g(\tau)\, d\tau}{1 + i\omega\tau} \tag{3}$$

with $\int_0^\infty g(\tau)\, d\tau = 1$. This expression gives the real and imaginary parts as

$$C'(\omega) = C_\mu \int_0^\infty \frac{g(\tau)\, d\tau}{1 + \omega^2\tau^2} \tag{4}$$

$$C''(\omega) = C_\mu \int_0^\infty \frac{\omega\tau g(\tau)\, d\tau}{1 + \omega^2\tau^2} \tag{5}$$

Equation 4 assures that C_μ is the low-frequency limit of C' when $\omega \to 0$. For experimental data fitting purposes, it is useful to reduce the freedom degrees of $g(\tau)$ to a function with a smaller number of parameters. One simple possibility is using a Cole−Cole equation that allows modeling it in terms of

dx.doi.org/10.1021/jp412641v | J. Phys. Chem. C 2014, 118, 6069−6076

individual circuit elements commonly integrated into fitting software packages

$$C(\omega) = C_\mu \frac{1}{1 + (i\omega\tau_c)^{1-\alpha}} \quad (6)$$

The parameter α ($0 < \alpha < 1$) accounts for the broadening of the conversion time distribution being $\alpha = 0$ the limit of a single relaxation time. τ_c marks the center of $g(\tau)$ and obviously correlates with the frequency of C'' peak as $\tau_c = 1/2\pi f_c$. The distribution function corresponding to eq 6 is symmetrical with respect to ln τ_c, and it resembles a Gaussian-like distribution concentrated around $-2 < \ln(\tau/\tau_c) < 2$. Therefore, the shape of C'' will be also symmetric around the peak.

The distribution width parameter α can be related to the so-called constant phase circuit element (CPE). Its impedance is given by the expression

$$Z_{CPE} = \frac{1}{Q(i\omega)^\alpha} \quad (7)$$

that, connected in series with a capacitor C_0, gives rise to the following complex capacitance function

$$C(\omega) = \frac{C_0}{1 + C_0 Q^{-1}(i\omega)^{1-\alpha}} \quad (8)$$

The comparison of eqs 6 and 8 allows identifying $C_0 = C_\mu$ and

$$\tau_c = \left(\frac{C_0}{Q}\right)^{1/(1-\alpha)} \quad (9)$$

Now, the limiting case $\alpha = 0$ is assimilated to the single conversion time case, and the CPE becomes a purely resistive circuit element. The conversion time in eq 9 allows defining an effective conversion resistance accounting for the overall resistive contribution of the reaction as

$$R_c = \frac{\tau_c}{C_\mu} \quad (10)$$

From the previous electrical modeling the whole equivalent circuit to be used for the electrode characterization comprises two subcircuits: (i) responding at high frequencies, C_{dl} in parallel with R_{ct} connected to the solution series resistance R_s; (ii) at low frequencies, conversion circuits accounting for each reaction observed in C'' spectra and represented by the series combination of the chemical capacitor and a CPE. This is summarized in the equivalent circuit in Figure 6 valid for the studied electrodes. It is noted here that two capacitive processes have been identified. We then denote as conversion process the mechanism that yields larger chemical capacitances C_μ^c and lower reaction frequencies f_c. The minor process observed at high-potential range is identified as prelithiation process producing much lower capacitances C_μ^l but higher reaction frequencies f_l.

A comparison between experimental data and fitting can be observed in Figures 3 and 4. It is known that Nyquist plots in Figure 3 highlight impedance features; thereby, resistive contributions to the overall response can be distinguished. Good fits are obtained in this representation that separates high-frequency interfacial circuit elements from low-frequency conversion mechanisms. Reaction features are properly displayed using the capacitance spectra of Figure 4. By examining Figure 4a, one can observe that the simple capacitance model in eq 8 is able to capture the essential features of C''. The frequency location of the conversion peak is clearly situated as well as the dispersion caused by $g(\tau)$.

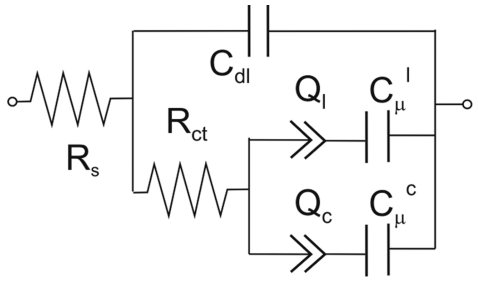

Figure 6. Equivalent circuit used for fitting. R_s is the series resistance, R_{ct} the interfacial charge-transfer resistance that combined with the double-layer capacitance C_{dl} dominates the high-frequency response. Reaction subcircuits are modeled by series CPE capacitance. C_μ accounts for the chemical capacitance of lithium in intermediate (l) Li–Zn–Fe–O and final (c) phases. The reaction retardation is assimilated into the CPEs Q_l and Q_c.

Discrepancies between experimental C'' data and the model in eq 6 are however visible in Figure 4b,c. This is caused by the lack of generality of the capacitance expression that imposes a drastic constraint concerning the symmetry of the conversion time distribution. It is known that more general models with asymmetric distribution tails can be devised, although this makes the fitting analysis much more complex. We have adopted here a compromise between model simplicity and reliable parameter extraction with the idea of capturing the most relevant information about the conversion kinetics.

DISCUSSION

Fitting results using the equivalent circuit of Figure 6 are summarized in Figure 7. By examining Figure 7a, one can observe chemical capacitance values for both processes. At lower potential, intermediate lithiation is masked by the huge C_μ^c values exhibited by the conversion process. In both cases, a rather monotonic increment occurs toward lower potentials being $C_\mu^c > C_\mu^l$ at a given potential. It is interesting to compare here the capacitance extracted from EIS with the discharge curve derivative $-dQ/dU$ of the second scan data in Figure 1b. After taking into consideration the electrode mass loading, this procedure and the capacitance can be directly confronted. Figure 7a allows inferring that while the discharge curve derivative is reduced at potentials below the peak at 1.0 V (which corresponds to the voltage plateau), chemical capacitance exhibits higher values. This discrepancy can be understood by considering that discharge curve at 40 mA g^{-1} (C/20 rate) is still far from equilibrium. On the contrary, EIS is measured in open circuit under negligible direct current flowing, which implies that capacitance extraction approximates equilibrium conditions.[24] This would entail that the discharge curve plateau prolongs in the case of ultraslow rates giving as a consequence increasing capacitances (curve derivatives) toward lower potentials. It is then conceivable that the sloping curve following the conversion plateau in Figure 1b is connected to a retardation effect of the reaction kinetics.

The reaction frequencies f_c and f_l calculated from the fitting parameters for conversion and prelithiation reactions, are plotted in Figure 7b. As previously observed in Figure 4b,c, the frequency corresponding to the C'' peak reaches a maximum at 1.0 V for the conversion mechanism and decreases monotonically at higher and lower potentials. Remarkably, the maximum

dx.doi.org/10.1021/jp412641v | J. Phys. Chem. C 2014, 118, 6069–6076

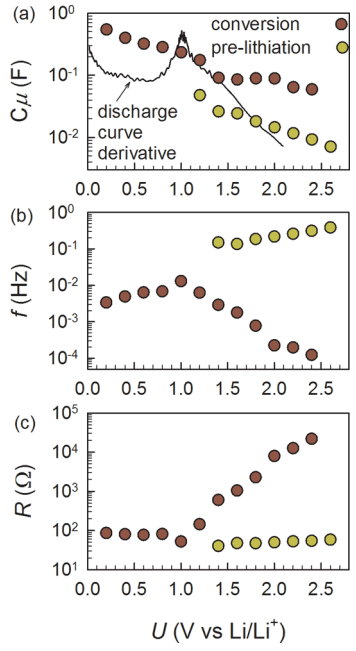

Figure 7. Fitting results using the equivalent circuit of Figure 6 showing (a) chemical capacitance C_μ, (b) reaction frequency f, and (c) reaction equivalent resistance R for the prelithiation Li−Zn−Fe−O phases formation, and the main conversion-alloying mechanism. In (a) solid line corresponds to the derivative of the discharge curve $-dQ/dU$ in Figure 1b considering the electrode mass loading.

conversion rate is reached at potentials (∼1.0 V) corresponding to the voltage plateau observed in the galvanostatic discharging experiment of Figure 1b. As commented upon previously, there is a retardation effect in the reaction kinetics below 1.0 V evidenced by the decreasing values reported for f_c. It is also noticeable that conversion frequency f_c is significantly lower than f_l. This would entail that the formation of intermediate Li−Zn−Fe−O phases is kinetically favored. Intermediate phases might then be seen as a sort of Li reservoir to be consumed by the much slower conversion reaction.

Kinetic limitations hindering each specific lithiation reaction can be alternatively inferred from the reaction resistance in Figure 7c. The resistance represents an average value accounting for overall reaction time distribution. The distribution parameter α defined in eq 7 lies within the range of 0.2−0.3, signaling a slightly dispersive reaction time. At potentials higher than 1.0 V conversion resistance R_c exhibits increasing values within the range of 100 Ω−22 kΩ, in good agreement with the resistive increment in addition to $R_s + R_{ct}$ observed in Figure 3. In the low potential range (<1.0 V) R_c practically yields a constant value around 80 Ω exhibiting a minimum of 52 Ω at 1.0 V. Lithiation involving intermediate phases produce a low resistance $R_l \approx 50$ Ω. As in the case of the reaction frequencies, $R_l < R_c$ in the high potential range, a result that again informs on the favored kinetics of the prelithiation reaction.

Capacitive analysis allows distinguishing two separated reaction processes that we have identified as originated by the prelithiation producing intermediate Li−Zn−Fe−O and the main conversion reaction at low potentials. As discussed previously, an additional reaction was proposed accounting for the extra specific capacity increase caused by the LiZn alloy formation.[10] It should be noted here that the distinction of the alloying reaction was made during the first lithiation step that made up a fully amorphous phase consisting of highly dispersed LiZn and Fe^0 in an amorphous Li_2O matrix. After the subsequent delithiation sweep, the formation of ZnO and Fe_2O_3 appears likely (see Figure 2), but a mixture of ZnO, Fe_2O_3, and $Zn_xFe_{2+x}O_4$ ($x \leq 1$) is also conceivable, although the definite structural composition in the charged (delithiated) state is not yet fully understood. Since the impedance measurements have been performed after a few lithiation/delithiation cycles, it is probable that the kinetic separation between LiZn alloying and conversion of the metal oxides into Li_2O is not accessible. This would explain why a unique C'' peak is observable at low potentials.

It is worth noting here that the proposed model for the impedance/capacitance behavior establishes a conversion frequency that is connected to the underlying kinetic constants of the reaction. Diffusion terms are intentionally disregarded in such a way that inherent resistive loss elements originate in the process of surpassing microscopic potential barriers defined by the reaction itself. It is otherwise recognized that microscopic models should include the inherent structural rearrangement occurring during the conversion and the energy losses involved in it. This is indeed a complex problem that would involve energetic, entropic, and mechanical terms in the definition of the Li chemical potential as a driving force for the conversion reaction progress.[25,26] There are still some open issues as the hysteretic behavior observed in Figure 1b which exhibits a voltage offset larger than 0.5 V between discharge and charge sweeps. Combined experimental information on the capacitive response and structural changes of other conversion materials is obviously needed to go further in this direction.

CONCLUSIONS

We remark that the performed analysis of the capacitance spectra produced by carbon-coated zinc ferrite anodes allows for a quantification of the kinetic parameters governing the various lithiation steps involved. A new equivalent circuit that directly models the conversion reaction process was set up by fitting the Nyquist and capacitance spectra plots from EIS analysis. The conversion reaction subcircuit is assimilated to a series RC and reproduces the main features in the discharge/charge voltage profile showing a maximum conversion frequency at plateau potentials. Prelithiation mechanisms related to the formation of intermediate Li−Zn−Fe−O phases are observed to be kinetically favored with respect to the main conversion reaction. This is evidenced by the values reached by the reaction frequency of the first lithiation process (150−400 mHz) in comparison with those observed for the main conversion in the range of 0.1−10 mHz. It is additionally proposed that the sloping curve following the conversion plateau in Figure 1b is connected to a retardation effect of the reaction kinetics. In summary, the analysis opens new room for understanding kinetic features of the lithiation process that are usually hidden by relying exclusively upon structural characterization techniques.

AUTHOR INFORMATION

Corresponding Author

*E-mail: garciag@fca.uji.es (G.G.-B.).

Notes

The authors declare no competing financial interest.

dx.doi.org/10.1021/jp412641v | J. Phys. Chem. C 2014, 118, 6069−6076

■ ACKNOWLEDGMENTS

We thank financial support from Generalitat Valenciana (ISIC/2012/008 Institute of Nanotechnologies for Clean Energies) and FP7 European project ORION (Large CP-IP 229036-2).

■ REFERENCES

(1) Tarascon, J. M.; Armand, M. Issues and Challenges Facing Rechargeable Lithium Batteries. *Nature* **2001**, *414*, 359−367.
(2) Choi, N.-S.; Chen, Z.; Freunberger, S. A.; Ji, X.; Sun, Y.-K.; Amine, K.; Yushin, G.; Nazar, L. F.; Cho, J.; Bruce, P. G. Challenges Facing Lithium Batteries and Electrical Double-Layer Capacitors. *Angew. Chem., Int. Ed.* **2012**, *51*, 9994−10024.
(3) Bresser, D.; Paillard, E.; Copley, M.; Bishop, P.; Winter, M.; Passerini, S. The Importance of "Going Nano" for High Power Battery Materials. *J. Power Sources* **2102**, *219*, 217−222.
(4) Cabana, J.; Monconduit, L.; Larcher, D.; Palacín, M. R. Beyond Intercalation-Based Li-Ion Batteries: The State of the Art and Challenges of Electrode Materials Reacting Through Conversion Reactions. *Adv. Energy Mater.* **2010**, *22*, E170−E192.
(5) Hu, Y.-Y.; Liu, Z.; Nam, K.-W.; Borkiewicz, O. J.; Cheng, J.; Hua, X.; Dunstan, M. T.; Yu, X.; Wiaderek, K. M.; Du, L.-S.; et al. Origin of Additional Capacities in Metal Oxide Lithium-Ion Battery Electrodes. *Nat. Mater.* **2013**, DOI: 10.1038/NMAT3784.
(6) Wang, F.; Robert, R.; Chernova, N. A.; Pereira, N.; Omenya, F.; Badway, F.; Hua, X.; Ruotolo, M.; Zhang, R.; Wu, L.; et al. Conversion Reaction Mechanisms in Lithium Ion Batteries: Study of the Binary Metal Fluoride Electrodes. *J. Am. Chem. Soc.* **2011**, *133*, 18828−18836.
(7) Khatib, R.; Dalverny, A.-L.; Saubanère, M.; Gaberscek, M.; Doublet, M.-L. Origin of the Voltage Hysteresis in the CoP Conversion Material for Li-Ion Batteries. *J. Phys. Chem. C* **2013**, *117*, 837−849.
(8) Bazant, M. Z. Theory of Chemical Kinetics and Charge Transfer Based on Nonequilibrium Thermodynamics. *Acc. Chem. Res.* **2013**, *46*, 1144−1160.
(9) Xu, C.; Zeng, Y.; Rui, X.; Zhu, J.; Tan, H.; Guerrero, A.; Toribio, J.; Bisquert, J.; Garcia-Belmonte, G.; Yan, Q. Amorphous Iron Oxyhydroxide Nanosheets: Synthesis, Li Storage, and Conversion Reaction Kinetics. *J. Phys. Chem. C* **2013**, *117*, 17462−17469.
(10) Bresser, D.; Paillard, E.; Kloepsch, R.; Krueger, S.; Fiedler, M.; Schmitz, R.; Baither, D.; Winter, M.; Passerini, S. Carbon Coated $ZnFe_2O_4$ Nanoparticles for Advanced Lithium-Ion Anodes. *Adv. Energy Mater.* **2013**, *3*, 513−523.
(11) Poizot, P.; Laruelle, S.; Grugeon, S.; Dupont, L.; Tarascon, J.-M. Nano-Sized Transition-Metal Oxides as Negative-Electrode Materials for Lithium-Ion Batteries. *Nature* **2000**, *407*, 496−499.
(12) Larchera, D.; Sudanta, G.; Lerichea, J.-B.; Chabreb, Y.; Tarascon, J.-M. The Electrochemical Reduction of Co_3O_4 in a Lithium Cell. *J. Electrochem. Soc.* **2002**, *149*, A234−A241.
(13) Lavela, P.; Tirado, J. L. $CoFe_2O_4$ and $NiFe_2O_4$ Synthesized by Sol−Gel Procedures for Their Use as Anode Materials for Li Ion Batteries. *J. Power Sources* **2007**, *172*, 379−387.
(14) Lavela, P.; Tirado, J. L.; Womes, M.; Jumas, J. C. Elucidation of Capacity Fading on $CoFe_2O_4$ Conversion Electrodes for Lithium Batteries Based on ^{57}Fe Mössbauer Spectroscopy. *J. Electrochem. Soc.* **2009**, *156*, A589−A594.
(15) Sharma, Y.; Sharma, N.; Subba Rao, G. V.; Chowdari, B. V. R. Li-Storage and Cyclability of Urea Combustion Derived $ZnFe_2O_4$ as Anode for Li-Ion Batteries. *Electrochim. Acta* **2008**, *53*, 2380−2385.
(16) Lavela, P.; Tirado, J. L.; Womes, M.; Jumas, J. C. ^{57}Fe Mössbauer Spectroscopy Study of the Electrochemical Reaction with Lithium of MFe_2O_4 (M = Co and Cu) Electrodes. *J. Phys. Chem. C* **2009**, *113*, 20081−20087.
(17) Reddy, M. V.; Yu, T.; Sow, C. H.; Shen, Z. X.; Lim, C. T.; Subba Rao, G. V.; Chowdari, B. V. R. α-Fe_2O_3 Nanoflakes as an Anode Material for Li-Ion Batteries. *Adv. Funct. Mater.* **2007**, *17*, 2792−2799.
(18) Bisquert, J. Chemical Capacitance of Nanostructured Semiconductors: Its Origin and Significance for Heterogeneous Solar Cells. *Phys. Chem. Chem. Phys.* **2003**, *5*, 5360−5364.
(19) Song, J.; Bazant, M. Z. Effects of Nanoparticle Geometry and Size Distribution on Diffusion Impedance of Battery Electrodes. *J. Electrochem. Soc.* **2013**, *160*, A15−A24.
(20) Levi, M. D.; Aurbach, D. Impedance of a Single Intercalation Particle and of Non-Homogeneous, Multilayered Porous Composite Electrodes for Li-Ion Batteries. *J. Phys. Chem. B* **2004**, *108*, 11693−11703.
(21) Meyers, J. P.; Doyle, M.; Darling, R. M.; Newman, J. The Impedance Response of a Porous Electrode Composed of Intercalation Particles. *J. Electrochem. Soc.* **2000**, *147*, 2930−2940.
(22) Garcia-Belmonte, G.; Bueno, P. R.; Fabregat-Santiago, F.; Bisquert, J. Relaxation Processes in the Coloration of Amorphous WO_3 Thin Films Studied by Combined Impedance and Electro-Optical Measurements. *J. Appl. Phys.* **2004**, *96*, 853−859.
(23) Böttcher, C. J. F.; Bordewijk, P. *Theory of Electric Polarization*; Elsevier: Amsterdam, 1978; Vol. 2.
(24) Liu, P.; Vajo, J. J.; Wang, J. S.; Li, W.; Liu, J. Thermodynamics and Kinetics of the Li/FeF_3 Reaction by Electrochemical Analysis. *J. Phys. Chem. C* **2012**, *116*, 6467−6473.
(25) Garcia-Belmonte, G.; García-Cañadas, J.; Bisquert, J. Correlation between Volume Change and Cell Voltage Variation with Composition for Lithium Intercalated Amorphous Films. *J. Phys. Chem. B* **2006**, *110*, 4514−4518.
(26) Levi, M. D.; Aurbach, D.; Maier, J. Electrochemically Driven First-Order Phase Transitions Caused by Elastic Responses of Ion-Insertion Electrodes under External Kinetic Control. *J. Electroanal. Chem.* **2008**, *624*, 251−261.